Proceedings of the 9th World Congress on Momentum, Heat and Mass Transfer (MHMT'24)
London, United kingdom – April 11 – 13, 2024
Paper No. ENFHT 331
DOI: 10.11159/enfht24.331

Experimental Research on Heat Conduction and Temperature Control Method in the Chamber of Large-Scale Geotechnical Centrifuge

Chuanxiang Zheng[1], Jinjie Lu[1], Shuang Wei[2], Wei Huang[3], Jiaming Yan[3], Yuchen Dai[1], Zhenyu Wang[1], Zhaobo Song[1], Jianqun Jiang[1]
[1]Institute of Process Equipment, Zhejiang University
No.38, Zheda Road, Hangzhou, China
zhchx@zju.edu.cn; lujinjie@szx2.onexmail.com; daiyuchenyc@126.com; zhenyuwang2020@zju.edu.cn; z_b_song@qq.com; jianqun@zju.edu.cn
[2]Hangzhou Chinen Turbine Co.,Ltd
No.18, 22nd Street, Hangzhou, China
18758569542@163.com
[3]Huadong Engineering Co.,Ltd
No.201, Gaojiao Road, Hangzhou, China
huang_w@hdec.com; yan_jm@hdec.com

Abstract **-** The high-speed rotation of the rotor in the large-scale geotechnical centrifuge generates significant heat due to air friction in the chamber, leading to an increase in temperature and affecting the normal operation of the machine and sensors. This paper conducted experiments and analysis on the heat conduction mechanism in the chamber of the super large-scale geotechnical centrifuge, as well as the theoretical analysis of heat dissipation methods for different heat sources. A scaled-down prototype model at a 1:15 ratio was designed to simulate the heat generation and dissipation caused by the friction of the high-speed rotor, and the reliability of the theoretical model was verified through testing. Based on this theoretical model, a temperature control method for the 1500g large-scale geotechnical centrifuge was proposed.

Keywords**:** Large-scale Geotechnical Centrifuge, Temperature Control, Wind Resistance Power, Vacuum

1. Introduction

The large-scale geotechnical centrifuge is a crucial tool for studying the spatiotemporal evolution of rock and soil, replicating geological processes, and accelerating the separation of substances. As the load capacity and centrifugal acceleration of the centrifuge increase, the time required to obtain test results decreases. Therefore, the trend is towards larger geotechnical centrifuges. One of the technical challenges in the process of scaling up is the threefold increase in wind resistance power with the increase in gravitational acceleration, leading to a rapid rise in chamber temperature and subsequent impact on the normal operation of the machine and sensors [1]–[4].

Temperature rise control Method is relatively straightforward at low centrifugal accelerations due to the small wind resistance power and easy heat dissipation. However, as the centrifugal acceleration exceeds 1000g, heat generation can reach megawatts, posing a challenge to temperature rise control. When the centrifugal acceleration exceeds 1500g, the wind resistance power can reach 10MW, resulting in an extremely severe temperature rise. Achieving temperature rise control at this point becomes a highly challenging problem [5], [6].

The largest geotechnical centrifuge in the world, produced by the American company Davis, can achieve a super-gravity acceleration of 1200g. Meanwhile, the largest geotechnical centrifuge under construction at Zhejiang University in China is designed to reach a super-gravity acceleration of 1500g and 1500g.T, with a 9m diameter and a maximum rotor linear velocity of 290m/s, making it the largest geotechnical centrifuge currently. The issue of temperature rise presents a significant challenge. This study aims to address the temperature rise control problem of large-scale geotechnical centrifuges above 1500g by investigating the heat generation mechanism of wind resistance power, proposing a novel temperature control method, and verifying the theoretical basis of heat dissipation through scaled model experiments [7]–[11].

2. Wind Resistance Power and Its Causes in Large-Scale Geotechnical Centrifuges

It is currently believed that the heat in geotechnical centrifuges mainly originates from the frictional heat generated by high-speed airflow rubbing against the walls. When high-speed airflow has a relative velocity with the metal surface, the shear friction force is produced at the boundary, and this force is converted into heat after doing work[12]–[19]. The greater the wind speed and the relative velocity with the metal, the greater the shear force and the more heat produced. The heat generated by the friction between air and the metal surface is divided into two parts. One part is the heat generated by the high-speed rotor rubbing against the air (referred to as the first heat), and the other part is the heat generated by the high-speed rotating air rubbing against the chamber wall surface (referred to as the second heat). This classification allows for the design of different cooling and heat dissipation systems based on the heat generated in different areas.

2.1. The Cause of Wind Resistance Power

Figure 1 illustrates the temperature distribution on the chamber wall of a geotechnical centrifuge when the linear velocity of the high-speed rotor reaches 290 m/s. It is observed that the side wall is the hottest area, indicating the highest heat generation in this region. The heat generation on the upper and lower walls decreases in a parabolic pattern along the radial direction, resulting in less heat generation on these surfaces. The following discussion primarily focuses on the theoretical and experimental research on controlling the temperature rise in the centrifuge, considering the mechanism of heat generation in the centrifuge chamber, the distribution of heat, and the heat dissipation.

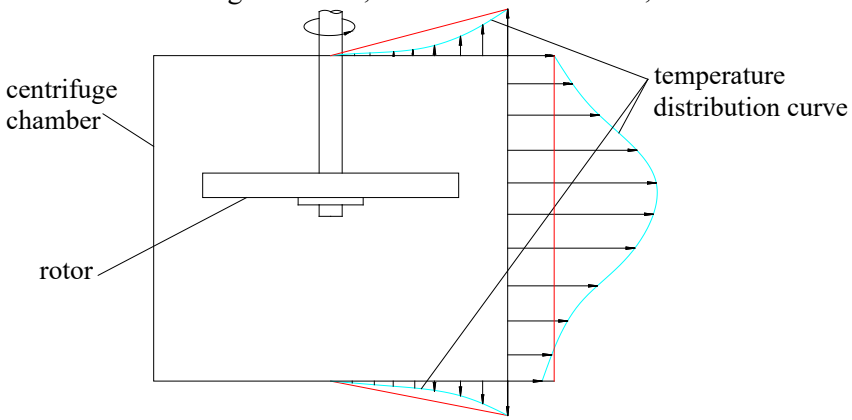

Fig. 1: Wall temperature distribution of a large-scale geotechnical centrifuge.

2.2. Calculation of Theoretical Wind Resistance Power

2.2.1. Existing Methods for Calculating Wind Resistance Power

Wind resistance power is the primary source of heat inside the geotechnical centrifuge. Due to the limited gas weight inside the chamber, most of the motor input power is converted into heat while overcoming wind resistance, with only a small portion being transformed into gas kinetic energy. Therefore, this paper analyzes and calculates the wind resistance power as the heat generated inside the chamber. Under this assumption, the motor input torque is assumed to be equal to the torque generated by gas and metal friction and shear forces. The following calculation formula is based on this assumption.

Internationally, there are several main calculation formulas for the wind resistance power (P_{w}) of large-scale geotechnical centrifuges. First, there is the calculation method from Actronic company in France[20]:

$$P_{\mathrm{w}} = \rho S_{\mathrm{n}} C_{\mathrm{x}} \omega (\omega R - V_{\mathrm{v}})^2 / 2 \tag{1}$$

Where C_{x} represents the modified effective wind resistance coefficient, ρ is the density of gas, S_{n} is the windward area of the rotor, ω is the rotational speed, R stands for the radius of the centrifuge, and V_{v} represents the circumferential linear velocity of the flowing gas. The same symbols below have the same definitions.

Calculation method from the China Academy of Engineering Physics[21], [22]:

$$P_{\mathrm{w}} = \rho C(1-\alpha)^2\omega^3\Psi/2 \tag{2}$$

Where α represents the relative coefficient with the flow, Ψ represents the velocity decay coefficient, and C represents represents the wind resistance coefficient.

Calculation method from Davis in the United States[20]:

$$P_{\mathrm{w}} = \rho(B_1(1-\alpha)^2\omega^3 - B_2\alpha^2\omega^3) \tag{3}$$

Where B_1 and B_2 represent torque coefficients, which can be calculated or experimentally determined based on geometric dimensions.

The calculation of wind resistance power above does not differentiate the heat generation components of each part, it only provides a total power value. To precisely design the heat dissipation system, it is essential to conduct separate heat dissipation designs for the different heat generation components.

2.2.2. Calculation of Heat Generation in Different Parts

To design an efficient heat sink, it is crucial to identify the location and size of the main heat sources. The primary heat generation is due to the shear force between high-speed airflow and the surfaces inside the chamber, resulting in heat generation by the work done on the solid surface. Based on this, a heat generation formula can be derived using the chamber's geometric dimensions and the flow ratio. It is assumed that the side wall airflow velocity is uniform, and the airflow velocity distribution on the upper and lower wall surfaces is linear, as indicated by the red line in Figure 1. The heat generation on each surface is calculated as follows:

$$M_{\mathrm{topwall}} = \int_0^R C_{\mathrm{fd}}\frac{\rho\alpha^2\omega^2r^2}{2}2\pi r^2dr = \frac{1}{5}\rho\alpha^2\omega^2\pi C_{\mathrm{fd}}R^5 \tag{4}$$

$$M_{\mathrm{sidewall}} = C_{\mathrm{fc}}\frac{\rho\alpha^2\omega^2R^2}{2}2\pi R^2H = \rho\alpha^2\omega^2\pi C_{\mathrm{fc}}R^4H \tag{5}$$

$$M_{\mathrm{rotor}} = 2\int_0^{r_{\mathrm{b}}} C_{\mathrm{db}}\frac{\rho(1-\alpha)^2\omega^2r^2}{2}rhdr = \frac{1}{4}\rho(1-\alpha)^2\omega^2C_{\mathrm{db}}hr_{\mathrm{b}}^4 \tag{6}$$

Where r is the radial distance from the centre of the rotation axis in the flow field, C_{fd} is the wind resistance coefficient of the topwall, C_{fc} is the wind resistance coefficient of the sidewall, C_{db} is the wind resistance coefficient of the rotor basket, H is the height of the centrifuge, h is the height of the rotor, r_{b} is the radius of the rotor.

Since the airflow velocity is linear, the above integral can be simplified, and then multiplied by the rotational speed to obtain the following heat generation formula:

$$Q_1 = (1-\alpha)\omega M_{\mathrm{rotor}} = \rho(1-\alpha)^3\omega^3\left(C_{\mathrm{dd}}r_{\mathrm{d}}^3S_{\mathrm{d}} + \frac{1}{4}C_{\mathrm{db}}hr_{\mathrm{b}}^4\right) \tag{7}$$

$$Q_3 = 2\alpha\omega M_{\mathrm{topwall}} = \frac{2}{5}\rho\alpha^3\omega^3\pi C_{\mathrm{fd}}R^5 \tag{8}$$

$$Q_4 = \alpha\omega M_{\mathrm{sidewall}} = \rho\alpha^3\omega^3\pi C_{\mathrm{fc}}R^4H \tag{9}$$

$$P_{\mathrm{w}} = \omega M_{\mathrm{rotor}} = \frac{1}{4}\rho(1-\alpha)^2\omega^3C_{\mathrm{db}}hr_{\mathrm{b}}^4 \tag{10}$$

Where S_{d} is the area of the windward side of the rotor, C_{dd} is the wind resistance coefficient of the rotor.

The ratio of the first heat source Q_1 to the second heat source Q_2, which equals $Q_3 + Q_4$, is:

$$\frac{Q_1}{Q_2} = \frac{Q_1}{Q_3 + Q_4} \tag{11}$$

When the wind resistance coefficient is the same, the heat generation on each surface is influenced by factors such as density (ρ), rotational speed (ω), and flow ratio (α).

The calculations above are based on two assumptions: first, the wind speed distribution around the centrifuge chamber follows the red line distribution in Figure 1; second, the density distribution within the chamber is assumed to be uniform. However, in reality, the wind speed and density distributions around the chamber are non-uniform. These assumptions are acceptable when the wind speed and centrifugal acceleration are low, but they lead to significant errors when the centrifugal acceleration and wind speed increase [11]. The different heat source distributions also significantly impact the design requirements of the temperature control cooling system. For example, the dissipation of the first heat source (Q_1) requires overcoming air-side thermal resistance, wall surface thermal resistance, and cooling liquid-side thermal resistance, while the second heat source (Q_2) only needs to overcome wall surface thermal resistance and cooling liquid-side thermal resistance. Understanding the distribution of the two heat sources is crucial for achieving precise temperature control. To further clarify the real situation of the heat source distribution, the following analysis is based on experimental measurement results and CFD simulation results.

2.3. Distribution of Heat Generation

A 3D model was developed for CFD analysis of a geotechnical centrifuge with a maximum linear velocity of 290 m/s, a diameter of 9 meters, and a maximum load of 1500g. The flow field visualization in Figure 2 reveals a region of aggregation for temperature, density, and pressure in a ring-shaped cylinder area at the sidewall and bottom of the centrifuge bucket. This region serves as a focal point for heat transfer, and was treated as a virtual calculation model with appropriate simplifications and assumptions in the heat transfer calculation.

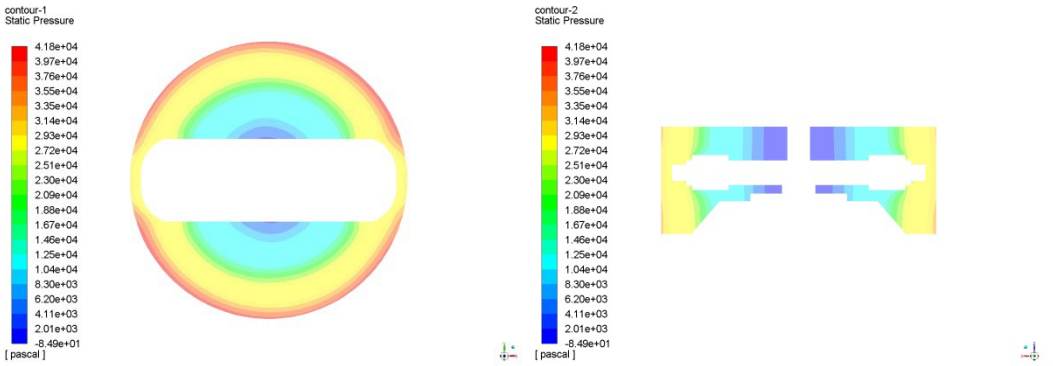

(a) Pressure contours

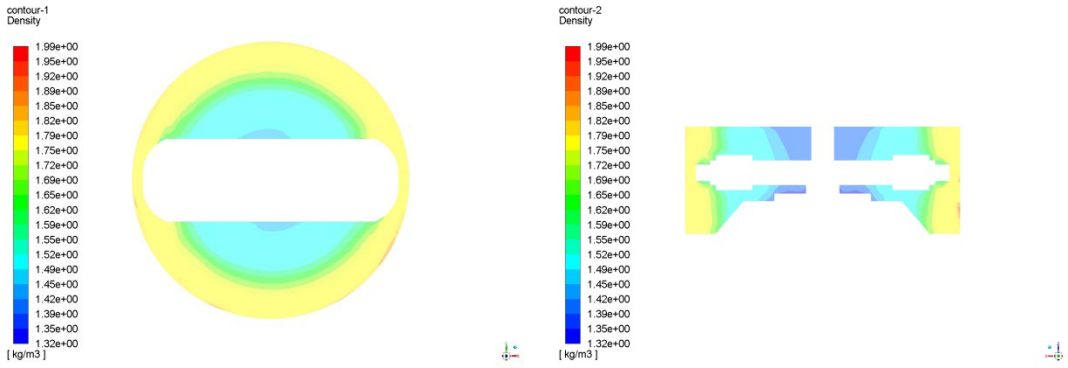

(b) Density contours

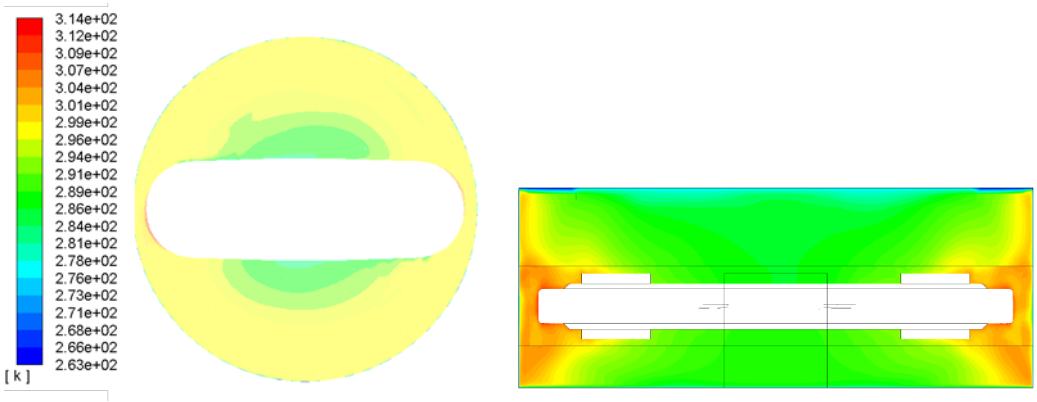

(c)Temperatur contours

Fig. 2: Numerical results from CFD simulation of the geotechnical centrifuge.

(1) Considering that the heat generation inside the centrifuge chamber is mainly caused by the heat generated from the friction between the rotor or the hoist with the air (Q_1), and the heat generated from the friction between the air and the centrifuge chamber wall (Q_2), other heat sources are negligible. The proportion of the two heat sources varies with the geometric dimensions of the chamber, and the proportion estimated by referencing the calculation method provided in reference [11] is taken as the maximum limit proportion, with some modifications made based on the experimental results.

(2) The rotating fluid inside the centrifuge is treated as an annular fluid rotating along the wall, with the inner wall of the annular fluid being the virtual diameter at the far end of the rotor, and the outer wall of the annular fluid enclosing the inner diameter of the chamber sidewall. The heat transfer calculation refers to the convective heat transfer in a circular pipe [23].

2.4. Analysis of Factors Influencing Wind Resistance Power

The calculation method for wind resistance power mentioned above indicates that the shape of the centrifuge rotor structure, chamber structure, surface smoothness of the centrifuge, air density, and rotor speed all influence wind resistance power. Once the chamber structure design is finalized, wind resistance power is only affected by rotor speed and fluid density within the chamber. When operating conditions are determined, it is solely related to fluid density. The primary factors influencing fluid density are temperature and pressure. Lowering the pressure and raising the temperature both result in reduced fluid density. Due to temperature constraints within the chamber, increasing the temperature is not feasible. Therefore, reducing pressure (creating a vacuum) is the most effective and commonly used method for reducing wind resistance power, and it has been widely adopted. Additionally, low-density gas can be used to replace air.

For a centrifuge with a small chamber and simple rotor structure, and reliable sealing, the evacuation process is undoubtedly a very suitable choice. However, for large-scale geotechnical centrifuges with a chamber diameter exceeding 9 meters and a complex structure, as well as the risk of lubricating oil leakage in bearings, the vacuum degree will be limited to a specific value, such as 1000 Pa. Increasing the vacuum degree further will have adverse effects on instruments, bearing lubrication systems, etc. In this case, it is necessary to consider using joint cooling methods other than vacuum extraction, such as the use of cooling liquid jackets.

3. Heat Transfer Theory Analysis

Based on the analysis of the heat generation mechanism and the spatial distribution of heat generation rate, targeted heat dissipation methods can be designed.

3.1. Heat Dissipation Mechanism

Under constant heat conditions in the centrifuge room, the geotechnical centrifuge can be considered as a cylindrical body with internal heat dissipation. By analyzing the temperature distribution inside the geotechnical centrifuge, heat sources and their respective heat dissipation paths can be determined. The first heat source (Q_1) dissipates heat air-side convection, metal wall conduction, and coolant-side convective heat exchange, with a substantial portion of this being removed through vacuum extraction. The second heat source (Q_2) dissipates heat through side wall metal conduction and coolant-side convective heat exchange, and reducing the side wall temperature accelerates the dissipation of this heat. Therefore, effective heat dissipation measures for structures like the geotechnical centrifuge include cooling the side walls, natural cooling of the upper and lower walls, and a combined vacuum extraction and temperature control inside the chamber. The following section presents the calculation and analysis of heat transfer for different heat dissipation paths.

3.2. The Heat Transfer Calculation Model

Based on the assumptions above, the heat transfer calculation for the centrifuge chamber can be conducted. The chamber is treated as a circular tube, and the gas inside is considered as a high-speed fluid in an annular gap. Heat is generated by the friction between the high-speed fluid and the wall, leading to forced convection heat transfer. The heat transfer calculation is based on a simplified formula for forced convection in a circular tube with the same Reynolds number as the fluid contact surface [23], and the heat transfer coefficient is then calculated. The main difference from the traditional circular tube convection heat transfer formula is that the fluid in the circular tube flows axially, whereas in the centrifuge, the fluid flows circumferentially. However, the relative flow velocity at the boundary remains the same.

3.3. Calculation of Heat Transfer Coefficient

The centrifuge chamber has a radius of R, a height of H, and a rotor speed of ω. The radial gap Δ refers to the gap between the outer side of the rotor end face and the inner surface of the chamber side wall. The outer diameter of the rotor is d, the height of the rotor is h, and the air velocity decay coefficient is represented by ψ. The total heat exchange area on the side is denoted as A. Based on the above calculation model, the heat transfer coefficients of each part can be calculated as follows:

① Calculation of the convective heat transfer coefficient between air and the tube wall

The airflow in the centrifuge chamber exhibits annular gap flow due to the rotation of the rotor. The outer side of the annular gap corresponds to the inner side of a circular tube with an inner diameter of D. The inner side of the annular gap corresponds to the outer side of a virtual circular tube, with an outer diameter of 470mm for the rotor, calculated based on a gap of 65mm. The equivalent diameter of this annular gap is:

$$d_e = \frac{4 \times H \times \frac{D-d}{2}}{2\ (H+\ (D\text{-}d)/2)} \tag{12}$$

Calculation of Reynolds number:

$$Re = \frac{u d_e \rho}{\mu} \tag{13}$$

Where u is the velocity of gas, μ is the dynamic viscosity of gas.

Calculation of Prandtl number:

$$Pr = \frac{c_p \mu}{\lambda} \tag{14}$$

Where c_p is the specific heat capacity, λ is the thermal conductivity.

Calculation of Nusselt number:

$$Nu=0.023Re^{0.8}Pr^{0.33} \tag{15}$$

Calculation of convective heat transfer coefficient for air-tube wall:

$$k_1=\frac{\lambda}{d_e}Nu \tag{16}$$

② Calculation of conduction heat transfer coefficient on the inner wall of the heat exchanger

$$k_2=\frac{\lambda}{\delta} \tag{17}$$

Where δ is the wall thickness.

③ Calculation of convective heat transfer coefficient for coolant-tube wall

$$k_3=0.027\left(\frac{\lambda}{d_e}\right)Re^{0.8}Pr^{0.33}\left(V_{is}^{0.14}\left[1+3.5\left(\frac{d_e}{D_c}\right)\right]\right) \tag{18}$$

Where d_e represents the equivalent diameter of the helical jacket, which is four times the jacket spacing. V_{is} is the ratio of the fluid viscosity at the bulk temperature to that at the wall temperature. Since the resistance due to the wall temperature can be neglected, V_{is} is taken as 1, and D_c is the mid-diameter of the jacket.

④ Total Heat Transfer Coefficient Calculation

The total heat transfer coefficient is calculated in two parts for different heat sources. The total heat transfer coefficient K_1 for the first heat source is calculated as follows:

$$K_1=\left(\frac{1}{k_1}+\frac{1}{k_2}+\frac{1}{k_3}\right)^{-1} \tag{19}$$

The total heat transfer coefficient K_2 for the second heat source is calculated as follows:

$$K_2=\left(\frac{1}{k_2}+\frac{1}{k_3}\right)^{-1} \tag{20}$$

After determining the logarithmic mean temperature difference of the cooling liquid, the parameters such as the size of the required cooler and vacuum degree can be designed based on the size of each heat source.

4. Experimental Research and Validation

For the current prototype of the large-scale geotechnical centrifuge, with a rotor linear velocity of 290m/s, a gravity acceleration of 1500g, and a chamber diameter of 9m, there is no precise method for calculating heat production and dissipation. Also, there are no existing centrifuges with such high acceleration and linear velocity for reference, and the scaling of centrifuges does not have a simple formula for enlargement. In order to verify the reliability of the calculation model, a simulation experimental device for the prototype machine was specifically designed for verification. The purpose of this verification is to confirm the accuracy of the simulation calculations for heat production and dissipation under the same maximum rotor linear velocity (i.e., under the same frictional shear force), and to verify the relationship between vacuum degree and temperature rise.

4.1. Experimental Principles and Apparatus

The prototype of the large-scale geotechnical centrifuge was scaled down to construct a model with a chamber 1:15 of the original prototype. The chamber diameter of the simulated centrifuge is 0.6 meters, and the outer diameter high-speed rotor is 470mm. The working process of the simulated centrifuge is illustrated in Figure 3, and the simulated centrifuge structure is shown in Figure 4. The experimental conditions include a spiral jacket with a -15°C ethylene solution on the sidewall, and the requirement is that the highest temperature inside the chamber does not exceed 40±5°C. The test condition involves a high-speed rotation of 11810rpm (equivalent to 290m/s).

At the beginning of the experiment, start the vacuum pump to evacuate the chamber to the set vacuum degree. After maintaining this vacuum degree for a period of time, start the motor to achieve a linear velocity of 290 m/s for the high-speed rotor. During the friction between the high-speed rotor and the air, heat is generated. When the temperature inside the chamber begins to rise as detected by the temperature sensor, the refrigeration unit is activated to inject the refrigerant into the liquid-cooled jacket. Once the heat generated by the wind resistance power reaches a balance with the heat dissipated by the cooling liquid, the temperature inside the chamber will stabilize. At this point, record the readings of the flow meter, the outlet and inlet temperatures of the cooling liquid, the input power of the motor, the air temperature at the upper, middle, and lower parts of the inner wall of the chamber, and the surface temperature at the upper, middle, and lower parts. Based on the recorded data, the heat Q_1 generated by the friction between the high-speed rotor and the air can be calculated.

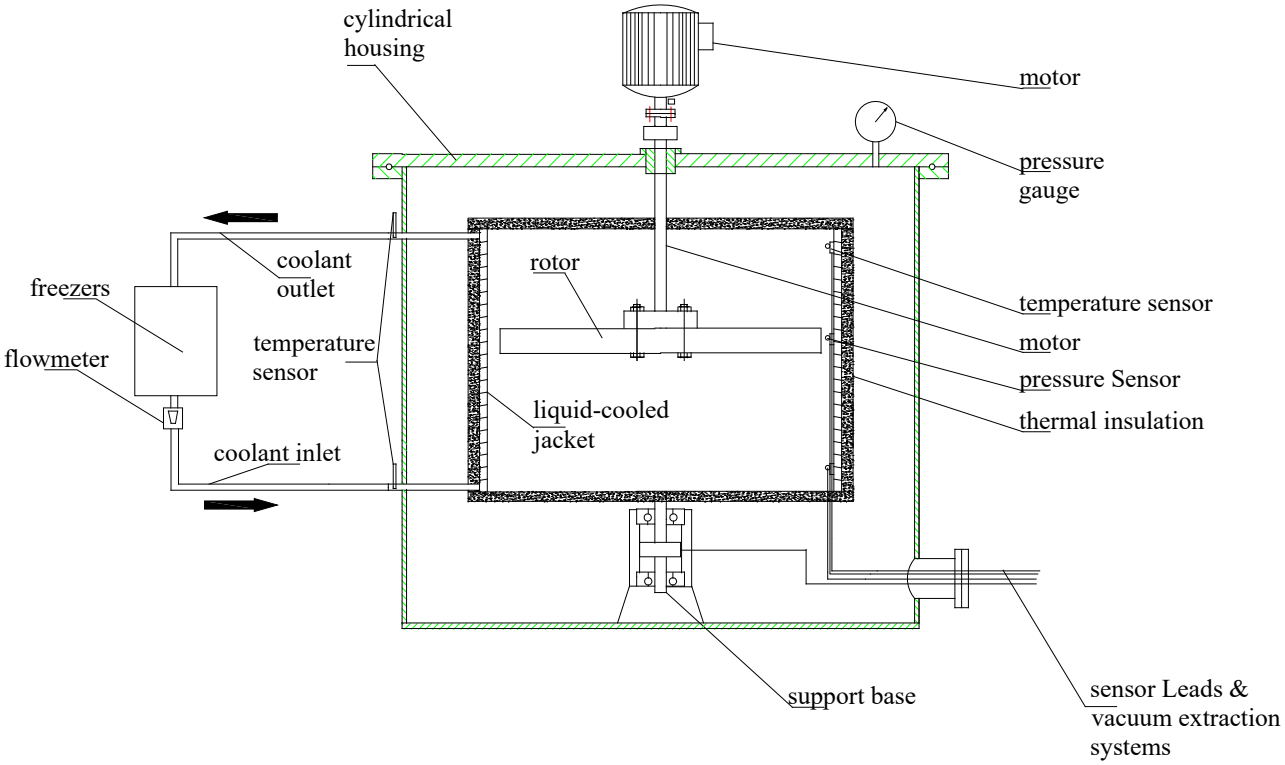

Fig.3: Wind resistance power test schematic.

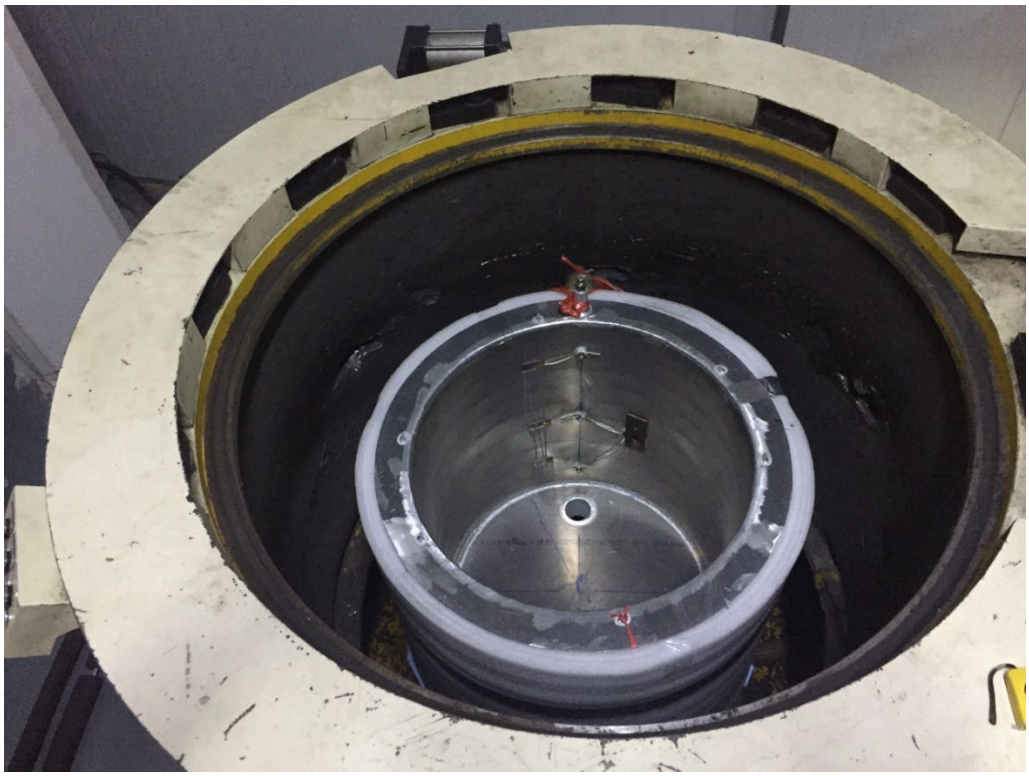

Fig. 4: Simulated centrifuge test device

4.2. Experimental Results and Discussion

Temperature test points were positioned at various locations within the simulated centrifuge chamber. The air temperature was found to be highest at the elevation where the high-speed rotor is located, and the chamber's highest temperature point varies with air pressure, as illustrated in Figure 1. At this point, the relative velocity between the rotor and the wall is 290m/s. The temperature distribution along the height of the side wall is detailed in Table 1.

Table 1: Experimental parameter record form of simulated centrifuge.

p/Pa / Time/min	1000Pa	3000Pa	5000Pa	10000Pa
1	5.4	-2.2	-0.6	4.5
2	15.6	0.9	3.5	11.8
3	32.8	13.8	18.8	24.9
4	39.1	34.0	36.9	45.7
5	40.5	39.7	45.4	50.3
6	41.2	41.0	46.3	51.1
7	41.5	41.6	46.9	51.4
8	41.7	41.8	47.3	51.9
9	41.9	42.1	47.6	52.1
10	40.3	42.3	47.8	52.3
11	38.5	42.6	48.0	52.4
12	37.3	42.8	48.2	52.6
13	36.8	43.0	48.3	52.7

14	36.5	43.3	48.4	52.8
15	36.4	43.4	48.6	52.8
16	36.5	43.5	48.8	52.9
17	36.5	43.7	49.0	53.0
18	36.5	43.7	49.1	53.1
19		43.8	49.1	53.2
20		43.9	49.3	53.3
21		44.3	49.4	53.4
22		44.4	49.4	53.4
23		44.5	49.4	53.4
24		44.5	49.4	53.4
25		44.5	49.4	53.4
26		44.6	49.4	53.4
27		44.7	49.4	53.5
28		44.7	49.4	
29		44.7		
30		44.9		
31		45.0		
32		45.1		
33		45.1		
34		45.1		

4.2.1. Verification of Heat Source Proportion

The main purpose of this experiment is to verify the control of temperature rise in the geotechnical centrifuge by increasing the combination of cooling jackets under a certain vacuum degree. The proportions of each heat source were also measured.

In the experiment, because the temperature on the liquid cooling side did not reach the required steady -15℃ at the inlet and -10℃ at the outlet, the measured quantity was the total heat dissipation. The total heat transfer quantity Q was calculated based on the measurements of the wall and liquid cooling side temperatures. Subsequently, Q_1 was calculated using the heat transfer coefficient k_1 on the air side and the average temperature difference between the air and the wall, resulting in $Q_2 = Q - Q_1$.

Using the above calculation method, the convective heat dissipation of the simulated centrifuge was calculated under the condition of 290m/s and 3000 Pa(A) air pressure. The actual measured average temperature of the centrifuge chamber air, the average wall temperature, and the actual inlet and outlet temperatures of the cooling liquid were used as the basis for the calculation.

Q_1 at 3000 Pa(A) in the simulated centrifuge:

$$Q_1 = k_1 * \Delta t_{m1} * A = 24.3 \times 26 \times 1.13/1000 = 0.71KW$$

Total amount of heat dissipation Q:

$$Q = K_2 * \Delta t_{m2} * A = 238.5 \times 18.34 \times 1.13/1000 = 5.02KW$$

Therefore, the heat dissipation of the second heat source Q_2 is:

$$Q_2 = Q - Q_1 = 5.02 - 0.71 = 4.31KW$$

Simultaneously, the heat generated by the wind resistance power carried away by the cooling liquid can be calculated using the flow rate and temperature difference on the cooling liquid side. The formula for this calculation is $Q_L = cq\Delta t$, where c represents the specific heat, q represents the mass flow rate of the cooling liquid, which is 0.238 kg/s, Δt is the temperature difference.

4.2.2. Temperature Control Method

The experimental results indicate that as the air pressure inside the chamber decreases, the maximum temperature inside inside the chamber also decreases. When the temperature of the side wall cooling liquid decreases, the temperature inside the chamber also decreases. Therefore, the method for achieving temperature control can be either vacuum extraction or low- or low-temperature side wall cooling, or a combination of both.

Considering the efficiency ratio of the centrifuge vacuum degree and the low-temperature method, ideal temperature control can be achieved with side wall cooling at -15°C when a high vacuum degree is used. When achieving the desired vacuum degree is challenging, temperature control can be achieved by further reducing the temperature difference of the side wall. The curve for temperature control of the centrifuge chamber with different pressures and low-temperature side wall cooling can be designed according to actual needs. Table 1 presents one of the vacuum degrees that achieve temperature control at a certain side wall temperature, and it also provides the side wall temperature that achieves temperature control at the set vacuum degree

5. Conclusion

By analyzing the heat generation mechanism of the large-scale geotechnical centrifuge, a heat dissipation temperature control method for the centrifuge is proposed. This method was validated through scaled-down prototype simulations, leading to the following conclusions:

(1) The heat generation of the geotechnical centrifuge is primarily due to the friction between the air and the centrifuge chamber. The sidewall is the area with the most heat generation, termed as the first heat source. Additionally, the friction between the air and the rotor also contributes to heat generation, known as the second heat source. The heat generation of the two heat sources at 3000Pa was obtained through the simulation test of the centrifuge.

(2) Under fixed centrifuge structure and operating conditions, the heat generation is directly proportional to the air density, and the heat transfer coefficient of the second heat source is also positively correlated with the air density. Although vacuum reduces the heat generation of the geotechnical centrifuge, it also increases the difficulty of heat dissipation of the second heat source. To address this issue, the simulation centrifuge uses a low-temperature cooling jacket to increase the average temperature difference for heat transfer, achieving the purpose of temperature control.

(3) The experimental results of the simulation centrifuge have demonstrated that vacuum and the cooling jacket can effectively dissipate the heat generation at a linear velocity of 290m/s, providing a temperature control solution for the heat dissipation of the prototype machine. This can further lead to the design and experimental verification of a larger simulation centrifuge, such as a 1:3 scale prototype.

Acknowledgements

This project was funded by the Centrifugal Hypergravity and Interdisciplinary Experiment Facility (CHIEF).

References

[1] Y. Yin and L. Dou, 'Aerodynamic power of geotechnical centrifuge', in *Advanced Materials Research*, 2012, vol. 421, pp. 788–791.

[2] Y. Hao, Y. H. Yin, and Q. Wan, 'Wind Resistance and Flow Characteristic Analysis of Geotechnical Centrifuges Based on Computational Fluid Dynamics', in *19th International Conference on Finite Elements in Flow Problems*, Rome, 2016.

[3] W. Yongzh, 'Simplified calculation technique of steady-state wind resistance power for geotechnical centrifuge and optimization cooling design', *Earthquake Engineering and Engineering Dynamics*, vol. 34, no. S1, pp. 909-914. (in Chinese), 2014.

[4] S. KRISHNAIAH and D. N. SINGH, 'Centrifuge modeling of heat and mass transfer through soils', in *12th Asian Regional Conference on Soil Mechanics and Geotechnical Engineering*, Singapore, 2003, pp. 393–396.

[5] Ji. Xing, Y. Xing, and J. Liang, 'Development and Thoughts of Geotechnical Centrifuge Modeling', *Journal of Water Resources and Architectural Engineering*, vol. 3, no. 1, pp. 27-31. (in Chinese), 2005.

[6] D. Yan-Ling, 'Fundamental Design Principles of Large Geotechnical Centrifuge', *Chinese Jounal of Geotechnical Engineering*, no. 6, pp. 10-17. (in Chinese), 1993.
[7] Y. Wang, 'Study on design theory and key technology of large dynamic centrifuge', Institute of Engineering Mechanics, China Earthquake Administration, Haerbin, 2013.
[8] J. F. CORTE, 'Design of geotechnical centrifuges', in *Centrifugeuses, Equipements et Instrumentation*, Paris, 1988.
[9] Pu J., 'Development trend of the geotechnical centrifuge modeling test and application', *Chinese Jounal of Geotechnical Engineering*, no. 5, pp. 96-98. (in Chinese), 1996.
[10] W. Craig and W. H. Craig, 'Édouard Phillips (1821–89)and the idea of centrifuge modelling', *Géotechnique*, vol. 39, no. 4, pp. 697–700, Dec. 1989, doi: 10.1680/geot.1989.39.4.697.
[11] C. Zheng, J. Chen, J. Jiang, and W. Lin, 'Experimental study on heat generation mechanism of geotechnical centrifuge under different vacuum degrees', *Equipment Environmental Engineering*, vol. 17, no. 3, pp. 84-88. (in Chinese), Jan. 2020.
[12] Y. Hao, Y. Yin, Q. Wan, and Q. Li, 'Wind Resistance and Flow Field Characteristic Analysis of Geotechnical Centrifuges Based on CFD', *Equipment Environmental Engineering*, vol. 15, no. 2, pp. 52–56, in Chinese 2018.
[13] Y. DU, L. ZHU, L. HAN, L. RU, P. JIA, and W. WANG, 'LXJ-4-450 geotechnical centrifuge in Beijing', Rotterdam, 1994, pp. 35–39.
[14] S. Krishnaiah and D. Singh, 'Determination of Thermal Properties of Soils in a Geotechnical Centrifuge', *Journal of testing and evaluation*, vol. 34, no. 4, pp. 1–8, Jul. 2006.
[15] B. A. I. Bing and Z. Jian, 'Some advances in geotechnical centrifuge model test technology', *Dam Observation and Geotechnical Tests*, vol. 25, no. 1, pp. 36–42, 2001.
[16] M. Sawada, S. Nishimoto, and T. Okada, 'New Rapid Evaluation for Long-Term Behavior in Deep Geological Repository by Geotechnical Centrifuge—Part 2: Numerical Simulation of Model Tests in Isothermal Condition', *Rock Mechanics and Rock Engineering*, vol. 50, no. 1, pp. 159–169, Jan. 2017, doi: 10.1007/s00603-016-1061-6.
[17] Zheng C. *et al.*, 'Apparatus and method for testing air friction heat production of geotechnical centrifuge under vacuum environment', CN201810579061.6, 2023
[18] D.-S. Kim, N.-R. Kim, Y. W. Choo, and G.-C. Cho, 'A newly developed state-of-the-art geotechnical centrifuge in Korea', *KSCE JOURNAL OF CIVIL ENGINEERING*, vol. 17, no. 1, pp. 77–84, 2013, doi: 10.1007/s12205-013-1350-5.
[19] Y. Sun, X. Yuan, Y. Wang, and L. Chen, 'Latest progress of centrifugal shakers in NEES and developmental conception of domestic centrifugal shakers', *World Earthquake Engineering*, vol. 26, no. 1, pp. 31-39. (in Chinese), 2010.
[20] Y. Hao, Y.-H. Yin, Q. Wan, and Q.-S. Li, 'Comparative Study on Estimation Methods of Wind Resistance of Geotechnical Centrifuges', *Equipment Environmental Engineering*, vol. 15, no. 3, pp. 61-66. (in Chinese), 2018.
[21] Y.-H. Yin, Y.-D. Liu, X.-L. Wang, and S.-R. Yu, 'Calculations of load rotational moment and rating power of centrifuges with rotation arms', *Journal of Mechanical&Electrical Engineering*, vol. 28, no. 6, pp. 659-662. (in Chinese), 2011.
[22] Y. Yin, S. Yu, X. Feng, P. Huang, X. Wang, and Y. Zhao, 'Aerodynamic Power of Geotechnical Centrifuges with Closed Chamber', *Journal of Mianyang Normal University*, vol. 29, no. 2, pp. 1-5. (in Chinese), 2010.
[23] X. Hao and D. Duan, *Principles of Chemical Engineering*, 2nd edition. Beijing: Science Press, 2019.